Meteorol. Z. (Contrib. Atm. Sci.), Early Access DOI 10.1127/metz/2023/1183

Towards higher accuracy in wind farm deficit decay modelling – a comparison

Moritz Mauz[1*], Stefan Emeis[2], Frederick Hoeckh[1], Bram van Kesteren[1], Andreas Platis[1] and Jens Bange[1]

[1]Department of Geoscience, Environmental Physics, University of Tübingen, Tübingen, Germany
[2]Institute for Meteorology and Climate Research, Karlsruhe Institute of Technology, Garmisch-Partenkirchen, Germany

(Manuscript received December 12, 2022; in revised form July 13, 2023; accepted July 18, 2023)

Abstract

Wind farm wake behaviour and forecasting is gaining the importance recently. It is especially relevant in the German Bight where space for wind farm clusters is limited, and wind farm wake lengths of up to 60 km have been measured. In this investigation newly proposed simple wind farm far-field recovery analytical wake model called SWIFFR is compared to the analytical EFFWAKE (Emeis, 2010) (Efficiency and Wake) wind farm wake model and the established Frandsen model (Frandsen et al., 2006). The models in this study are compared to measured in-situ airborne data, captured during the WIPAFF (wind park far field) project. Three specific flights are shown and compared to the respective model result of each analytical model. The SWIFFR model is derived from the Reynolds-averaged Navier-Stokes equation for the momentum conservation. It describes the wind speed recovery, as for example, in the wake of a wind farm from an atmospheric point of view, by acknowledging turbulent momentum from the atmosphere aloft of the wind farm wake and from the sides as well. A gain in accuracy in comparison to the EFFWAKE model is achieved. Analytical models provide computationally inexpensive results based on some assumptions and simplifications of the governing equations, which distinguishes this approach from purely empirical models.

Keywords: wind energy, off-shore wind farms, wake recovery, airborne measurements, analytical model, turbulence

1 Introduction

Regenerative energy sources have become a reliable power source for many countries, while the share of fossil energy sources is declining. One of the main regenerative sources is wind energy harvesting. Wind turbines (WTs) are spread all over the countryside, often providing decentralised power to the existing grid. However, energy production is achieved more efficiently in off-shore wind farms. In the early days of off-shore wind farm design, the dominating focus was cost per turbine or cost per surface area, ignoring wakes, their lengths and recovery. Looking back, the first wind farms are not among the most efficient ones. The spacing of individual WTs has become an important aspect in wind farm design and a lot of effort has been put into research to find a realistic cost ratio and to define minimum distances between WTs (Meyers and Meneveau, 2012; Yang et al., 2012). While the individual wake of a WT in an off-shore wind farm received a lot of attention, experimental in-situ studies evaluating the entire off-shore wind farm wake have only be conducted recently. The WIPAFF (wind park far field) project (Platis et al., 2020b; Platis et al., 2020a; Emeis et al., 2016) provides a unique data set of in-situ wind farm wake measurements. The data were captured at different thermal atmospheric conditions. Wake lengths of up to 60 km were found in stable atmospheric conditions.

Siedersleben et al. (2018) studied large off-shore wind farms and their effect on local wind fields using WRF (weather research and forecast) models under various atmospheric conditions. Off-shore wind farms can be expected to influence the meso-scale wind field (Siedersleben et al., 2018) and a turbine-atmosphere interaction on on-shore wind farms has been documented recently (Antonini and Caldeira, 2021). For weather forecast and wind farm efficiency considerations, these meso-scalic effects need to be quantifiable. Also Zhan et al. (2020) confirmed wake variability for different atmospheric stabilities using lidar (light detection and ranging) measurements for an on-shore wind farm.

Emeis (2010) proposed a simple analytical model to describe the flow field behind an off-shore wind farm. The model describes an exponential decay of the wind deficit and introduces a constant wind deficit decay rate α. In the presented work WIPAFF data are compared against the analytical model (EFFWAKE) proposed by Emeis (2010); Emeis (2022). The EFFWAKE (Efficiency and wake) model (Emeis, 2022) is an easy to set up model. Yet, it lacks accuracy in the wake recovery and does not take into account the wind farm ge-

*Corresponding author: Moritz Mauz, Department of Geoscience, Environmental Physics, University of Tübingen, Germany, e-mail: moritz.mauz@uni-tuebingen.de

ometry (Platis et al., 2018). An unsolved problem of the EFFWAKE model is the determination of one of its key parameters; the separation height Δz that separates the wind farm wake from the undisturbed flow above (Platis et al., 2020a). The results in Emeis (2010); Emeis (2017) were obtained by putting $z/\Delta z = 2$, with z the hub height of the wind farm.

In general, the influence of the wind farm geometry (WT spacing and density) and lateral momentum influx along the wake need also to be accounted for in the determination of the wind farm wake decay (Platis et al., 2018). Thus, there are still some uncertainties influencing the wind deficit decay rate that the EFFWAKE model can not formally address, since it assumes an infinite lateral extent of the wind farm. Therefore, an analytical model that could estimate any wind farm wake, determined by a few parameters, would help to quantify wind farm wakes properly while using little computational capacities.

Canadillas et al. (2020) compared the WIPAFF data to a median exponential best fit of the EFFWAKE model and additionally to the engineering software suite 'WindFarmer' (Hassan and Partners Ltd., 2014) which provides a modified wind farm wake model (Katik et al., 1987; Jensen, 1983). The WindFarmer bottom-up modelled results were found to be adequate for the data measured in neutral conditions. For stable conditions the wake lengths were significantly underestimated (Canadillas et al., 2020). Canadillas et al. (2020) showed that the wind farm wake can be described by an exponential function, best-fitting unknown parameters of the EFFWAKE model.

With wind farm wakes up to 60–80 km length it is likely that wind farms will interfere with each other, if they are not planned accordingly. Thus, also considering commercial software suites, there is a need for an easy to implement model that accounts for atmospheric stability. The proposed SWIFFR model provides such an analytical solution for the recovery of a wind velocity depression, e.g. typically found behind farm wakes, derived from the momentum conservation equation of the free flow.

One advantage of the proposed top-down model is that this model provides an analytical solution, with one less unknown parameter (vertical separation height), compared to the EFFWAKE model. Another advantage is that the wind farm is treated like a 'black box', resulting in a wake centre-line, without the need to compute the wake for each single turbine in the wind farm (bottom-up approach) as shown e.g. in Niayifar and Porté-Agel (2016) or the quite popular Frandsen model (Frandsen et al., 2006). Frandsen et al. (2006) relates the wake velocity directly to the thrust coefficient C_T of the wind turbine. This model uses a wake expansion parameter k, to effectively calibrate the model. This parameter varies, depending on turbine spacing, boundary layer conditions and turbine dimensions. Hence, it is problematic and almost impossible to define a common expansion factor (Andersen et al., 2014). Simple top-down analytical solutions can circumvent such problems and are also interesting for meso-scale WRF simulations or quick wake length assessments. The proposed model can also be applied to estimate off-shore wind farm spacings and studying wind farm wake interactions and shadowing. It is shown below that the SWIFFR model can be used with several forms of parametrisation.

2 Theory and methods

2.1 The EFFWAKE model

In this study the wind farm wake model derived by Emeis (2010) is referred to as the EFFWAKE model. It has been used by Platis et al. (2018); Platis et al. (2020a) and Canadillas et al. (2020) to compare in-situ airborne wind farm wake measurements to an analytical model. A detailed derivation is given in Emeis (2010); Emeis (2017). Nevertheless, a brief introduction of the model is given below.

The model is using a semi-empirical approach and assumes a wind farm with an infinite lateral extent. The EFFWAKE model further assumes a homogeneous inflow along the infinite lateral extent of the wind farm and is based on an equilibrium between momentum dissipation by the wind farm and a resupply of momentum by turbulent fluxes from the layer atop. Therefore, the momentum influx that restores the kinetic energy back to the flow has to come from the airflow above the wind farm. For its derivation the EFFWAKE model considers an accelerating air parcel with its remaining or residual wind speed u_r along the wake at hub height.

$$\frac{\partial u_r}{\partial t} = -\frac{\partial \overline{u'w'}}{\partial z} \tag{2.1}$$

The Reynolds-averaged turbulent vertical momentum flux in mean wind direction (right side of Eq. 2.1), where the primes describe the fluctuation from the mean quantity, is substituted using a bulk parametrisation (gradient method), introducing a turbulent momentum transfer coefficient K_m which varies with height in the Prandtl layer, however it is assumed constant at hub height z:

$$\overline{u'w'} = -K_m \frac{u_0 - u_r}{\Delta z} \tag{2.2}$$

The free stream velocity u_0 aloft and in front of the wind park or wind turbine is separated by Δz from the hub height, the assumed vertical wake-centre line. Thus the momentum transfer takes place along a vertical distance Δz (s.a. Figure 1). Since only the two velocities u_r in the wake at hub height and u_0 in the free stream (above the wind farm) are assumed, distance differentials can be written as differences and a first order differential equation can be formed:

$$\frac{\partial u_r}{\partial t} + \frac{K_m}{\Delta z^2} u_r = \frac{K_m}{\Delta z^2} u_0, \tag{2.3}$$

which has the solution

$$u_r(t) = u_0 + c\ \exp\left(-\frac{K_m}{\Delta z^2}t\right). \tag{2.4}$$

Applying the initial conditions $u_r(t = 0) = u_{r0} = u_0 + c$ gives a time dependent solution for the normalised residual wind velocity $u_r(t)/u_0$ at hub height h:

$$\frac{u_r(t)}{u_0} = 1 + \left(\frac{u_{r0}}{u_0} - 1\right)\exp\left(-\alpha_{\mathrm{E}}t\right), \text{ with: } \alpha_{\mathrm{E}} = \frac{K_{\mathrm{m}}}{\Delta z^2} \tag{2.5}$$

Platis et al. (2020a) resolve the temporal dependency by substituting t with $\bar{t} = \frac{x_i}{u_{50\,\%}}$, which gives an average time of flight of an air parcel from the beginning of the wake to the position x_i in the wake. This parcel travels with an average velocity $u_{50\,\%}$ through the wake. This is also the velocity at which the wind deficit is recovered by 50 %. The wake deficit decay rate α_{E} (index E indicating the EFFWAKE wake deficit decay rate) is assumed constant along the wake with momentum transfer from $z = h + \Delta z$ aloft the wake. The atmospheric thermal stratification or stability influences K_m by the friction velocity u_* and a stability correction function ϕ_m, in the lower atmosphere (Garratt, 1994a).

$$K_m = \frac{\kappa u_* z}{\phi_m(z/L)} \tag{2.6}$$

While for a neutral stratification $\phi_m(z/L) = 1$ can be applied, for unstable and stable stratifications different corrections apply (Businger et al., 1971).

$$\phi_m\left(\frac{z}{L}\right) = \begin{cases} 1/\gamma & \text{for } \frac{z}{L} < 0 \\ 1 & \text{for } \frac{z}{L} = 0 \\ 1 + a\frac{z}{L} & \text{for } \frac{z}{L} > 0 \end{cases} \tag{2.7}$$

With $\gamma = (1 - b\ z/L)^{0.25}$ and L the Obukhov length, $a = 5$ and $b = 16$. A numerical modeller that has access to stability data could now insert a stability correction into the model. In the EFFWAKE model the atmospheric stability is represented by the stability correction function ϕ_m, if apprehensible. But since the ϕ_m stability correction is essentially a constant, it effectively simply weights the momentum transfer coefficient K_m (same as a change in Δz). Meaning that whenever the EFFWAKE model is tuned or set up, it is not distinguishable whether the stratification correction or the separation height Δz is adjusted. Thus, as Δz and the Obukhov length are not obtainable for the presented cases (e.g. lack of surface virtual potential temperature flux data), the EFFWAKE model will be used for $\phi_m = 1$. Both parameters influence the wind deficit decay rate α_{E}, and since the thermal stability also impacts the boundary layer aloft the wind farm, only Δz will later be modified to fit the EFFWAKE model to the data. This treats α_{E} as a 'black box', as done by Platis et al. (2020a).

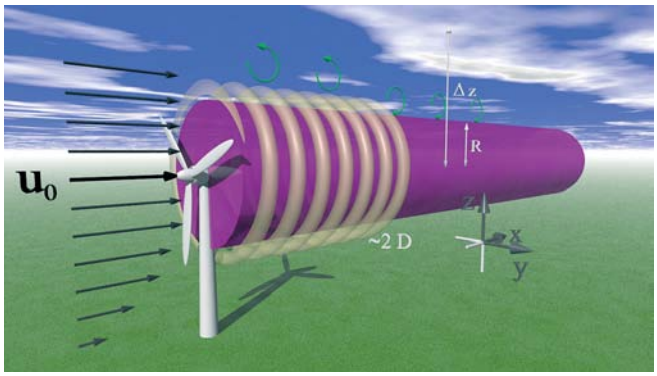

Figure 1: Wake characteristics displayed at a single turbine. The incoming horizontal wind u_0 ($= u_f|_{x=0}$) is almost steady over the rotor plane. The helical blade-tip vortex absorbs turbulent momentum flux from aloft, until the helix disintegrates (at $\approx$ 2D) and turbulent influx can refill the wake deficit. The EFFWAKE model assumes this distance to be Δz. Since this parameter is usually not determinable and unknown in the EFFWAKE model; the new proposed model approach uses the rotor radius R as the characteristic distance associated to the turbulent momentum influx.

Canadillas et al. (2020) tested the EFFWAKE model from an engineering point of view by calculating the initial wind velocity deficit u_{r0}/u_0 as a function of ambient turbulent intensity I_u, the farm thrust coefficient c_t, effective drag coefficient C_D and individual converter spacing (WTs per certain distance). For more details and the implementation the reader is referred to appendix B in Canadillas et al. (2020). In contrast to this full-on calculated wind farm wake, Platis et al. (2020a) substituted the initial wind deficit behind the wind farm u_{r0}/u_0 with a measured value from the WIPAFF campaign and compares the EFFWAKE model to these measured in-situ data.

Both studies described above, with different approaches, show a certain level of flexibility of the EFFWAKE model. A drawback of the EFFWAKE model is the unknown separation height parameter Δz. In the novel analytical model, presented in this work, this separation height is set fix to the rotor radius R of the wind turbines in the wind farm. It is used as a characteristic length associated to the wind farm wake, defining an altitude (boundary) above the wind farm through which all vertical momentum transfer has to transverse.

2.2 The SWIFFR model

For the SWIFFR (simple wind farm far-field recovery) model derivation we start with a flow around an offshore wind farm. Equation 2.8, the starting point for the newly proposed analytical wind deficit model, is the conservation of momentum in the incompressible mean flow using Einstein summation notation (Stull, 1988). After Reynolds averaging and applying the Boussinesq eddy viscosity assumption, the conservation of momen-

tum can be written as:

$$\underbrace{\frac{\partial \overline{u_i}}{\partial t}}_{\text{I}} + \underbrace{\overline{u}_j \frac{\partial \overline{u_i}}{\partial x_j}}_{\text{II}} + \underbrace{\delta_{i3} g}_{\text{III}} - \underbrace{f_c \epsilon_{ij3} \overline{u}_j}_{\text{IV}} + \underbrace{\frac{1}{\overline{\rho}} \frac{\partial \overline{p}}{\partial x_i}}_{\text{V}} - \underbrace{\frac{\nu \partial^2 \overline{u_i}}{\partial x_j^2}}_{\text{VI}} + \underbrace{\frac{\partial \overline{u_i' u_j'}}{\partial x_j}}_{\text{VII}} = 0 \quad (2.8)$$

Here, $i, j = 1, 2, 3$ for all three directions in space, g is the gravitational acceleration, p the static pressure, f_c the Coriolis parameter, ν the kinematic viscosity, ϵ the Levi-Civita symbol and ρ the density of air.

Term I represents storage of mean momentum.

Term II describes advection of mean momentum by the mean wind.

Term III allows gravity to act in the vertical direction only.

Term IV describes the influence of the Coriolis force.

Term V describes the mean pressure-gradient force.

Term VI represents the influence of viscous stress on the mean motions.

Term VII represents the influence of Reynolds stress on the mean motions.

Various terms in the Navier-Stokes equations can be neglected in boundary-layer flows with very low friction (Prandtl, 1904). Thus, assuming only very small changes in atmospheric pressure along the wind farm wake, term V can be neglected. Term VI represents the viscous stress but observations in the atmosphere indicate that the molecular diffusion is several order of magnitudes smaller compared to the other terms and can be neglected (Stull, 1988). Satellite imagery using synthetic aperture radar (SAR) show wake lengths up to 50 km and larger which show no to little deflection by Coriolis forces (Djath et al., 2018). Also for the sake of simplification term IV is neglected in this study. Considering only the wake-centre line of a one-dimensional ($i = 1$) steady-state flow, term I and III are zero and can also be deleted. Equation 2.8 can now be simplified. The mean reduced horizontal wind speed $\overline{u}$ in the wake at hub height in x-direction along the wake-centre line for an incompressible flow, with the remaining terms II and VII, can be approximated as:

$$\overline{u}\frac{\partial \overline{u}}{\partial x} + \overline{v}\frac{\partial \overline{u}}{\partial y} + \overline{w}\frac{\partial \overline{u}}{\partial z} = -\frac{\partial \overline{u'u'}}{\partial x} - \frac{\partial \overline{u'v'}}{\partial y} - \frac{\partial \overline{u'w'}}{\partial z} \quad (2.9)$$

Applying the product rule to each term on the left hand side of Eq. 2.9 yields:

$$\overline{u}\frac{\partial \overline{u}}{\partial x} = \frac{\partial \overline{u}^2}{\partial x} - \overline{u}\frac{\partial \overline{u}}{\partial x}; \quad (2.10)$$

$$\overline{v}\frac{\partial \overline{u}}{\partial y} = \frac{\partial (\overline{u}\,\overline{v})}{\partial y} - \overline{u}\frac{\partial \overline{v}}{\partial y}; \quad (2.11)$$

$$\overline{w}\frac{\partial \overline{u}}{\partial z} = \frac{\partial (\overline{u}\,\overline{w})}{\partial z} - \overline{u}\frac{\partial \overline{w}}{\partial z}; \quad (2.12)$$

The left side of Eq. 2.9 can now be rewritten as:

$$\begin{aligned} &\frac{\partial \overline{u}^2}{\partial x} - \overline{u}\frac{\partial \overline{u}}{\partial x} + \frac{\partial (\overline{u}\,\overline{v})}{\partial y} - \overline{u}\frac{\partial \overline{v}}{\partial y} + \frac{\partial (\overline{u}\,\overline{w})}{\partial z} - \overline{u}\frac{\partial \overline{w}}{\partial z} \\ &= \frac{\partial \overline{u}^2}{\partial x} + \frac{\partial (\overline{u}\,\overline{v})}{\partial y} + \frac{\partial (\overline{u}\,\overline{w})}{\partial z} - \overline{u}\underbrace{\left[\frac{\partial \overline{u}}{\partial x} + \frac{\partial \overline{v}}{\partial y} + \frac{\partial \overline{w}}{\partial z}\right]}_{=0} \end{aligned} \quad (2.13)$$

Since a steady-state incompressible flow is considered, the part in brackets in Eq. 2.13 is zero (divergence-free flow). The left side of Eq. 2.9 can now be written using Eq. 2.13, which results in Eq. 2.14:

$$\underbrace{\frac{\partial (u_r \cdot u_r)}{\partial x}}_{A} + \underbrace{\frac{\partial (\overline{v} \cdot u_r)}{\partial y}}_{B} + \underbrace{\frac{\partial (\overline{w} \cdot u_r)}{\partial z}}_{C} = \underbrace{-\frac{\partial (\overline{u'u'})}{\partial x}}_{D} \underbrace{-\frac{\partial (\overline{u'v'})}{\partial y}}_{E} \underbrace{-\frac{\partial (\overline{u'w'})}{\partial z}}_{F} \quad (2.14)$$

With $u_r = \overline{u}$ the reduced wind speed in the wind farm wake along the centre-line and the Reynolds shear stresses on the right-hand side.

Furthermore the continuity equation for incompressible steady-state flow is valid:

$$\frac{\partial v}{\partial y} + \frac{\partial w}{\partial z} = -\frac{\partial u_r}{\partial x} \quad (2.15)$$

The left hand side (term A, B and C) of Eq. 2.14 at the centre line can now be simplified using Eq. 2.15:

$$\begin{aligned} &\frac{\partial (u_r \cdot u_r)}{\partial x} + \underbrace{u_r \frac{\partial \overline{v}}{\partial y} + u_r \frac{\partial \overline{w}}{\partial z}}_{-u_r \frac{\partial u_r}{\partial x}} + \underbrace{\overline{v}\frac{\partial u_r}{\partial y}}_{=0} + \underbrace{\overline{w}\frac{\partial u_r}{\partial z}}_{=0} \\ &= 2u_r \frac{\partial u_r}{\partial x} - u_r \frac{\partial u_r}{\partial x} = u_r \frac{\partial u_r}{\partial x} = \frac{1}{2}\frac{\partial u_r^2}{\partial x} \end{aligned} \quad (2.16)$$

At the wake-centre line the mean lateral velocity component $\overline{v} = 0$ due to symmetry reasons. For simplicity, the same argument can be made for the vertical wind component $\overline{w}$, considering a homogenous rectangular cross-section of the wake (lateral).

Let us now consider the right-hand side (terms D, E and F) of Eq. 2.14. Concerning term D, it is common, to neglect this longitudinal change (i.e. in x-direction)

of the longitudinal turbulent flux of longitudinal momentum in comparison to $\partial u_r^2/\partial x$. The lateral Reynolds shear stress created by a WT in a wind farm is considered to be of same extent as the vertical shear stress due to the radial symmetry of the rotor plane. Thus, we can write:

$$\overline{u'v'} \approx \overline{u'w'} \tag{2.17}$$

Since furthermore a steady-state and stationary solution is considered, and no implicit dependencies of u are present, we use the total derivative instead of the partial. The remaining terms E and F of the right-hand side of Eq. 2.14 can therefore be rewritten:

$$-\frac{d\overline{u'w'}}{dy} - \frac{d\overline{u'w'}}{dz} = -\frac{d\overline{u'w'}}{f \cdot dz} - \frac{d\overline{u'w'}}{dz} = -\frac{d\overline{u'w'}}{dz}\left(\frac{1}{f} + 1\right) \tag{2.18}$$

With dy the lateral separation of the wind farm centre line from the free stream velocity u_0 and dz the vertical separation from the free stream velocity u_0. The lateral separation length is a manifold of dz, therefore $dy = f \cdot dz$, and since dz is the rotor blade length, for wind farms that consist of at least two rows of wind turbines along the wind direction $f > 1$. This introduces a way to recognise wind farm geometry when considering turbulent momentum influx into the wake from the sides affecting the wind deficit at the wake-centre line. Note that for the case of a single WT $dy = dz$ and therefore, $\frac{1}{f} + 1 = 2$, or $f = 1$ which would be the solution for the Reynolds stress terms for a single WT. Also, the wider a wind farm is built, the less prevalent is the lateral influx. The narrower a wind farm is built, the larger the influence of lateral momentum influx becomes.

The Reynolds shear stress is further simplified by an empirical relation (gradient method), assuming a first order distribution of the vertical Reynolds shear stress, s.a. Eq. 2.2. Therefore, the Reynolds shear stress is expressed using a momentum transfer coefficient K_m (s.a. Eq. 2.6) and is brought to a finite difference form at the wake-centre line at hub height h. In this approach we substitute Δz with the rotor length R, neglecting wake expansion:

$$\frac{d\overline{u'w'}}{dz} \rightarrow \frac{\Delta\overline{u'w'}}{R} = \frac{\overline{u'w'}(h + R/2) - \overline{u'w'}(h - R/2)}{R} \tag{2.19}$$

In order to obtain the flux-divergence at height h for all x, assuming a symmetric wake flow above and below the centre line, the resulting form is:

$$\begin{aligned}\frac{\Delta\overline{u'w'}}{R} &= -K_\mathrm{m}\frac{(u_0 - u_r)/R - (u_r - u_0)/R}{R} \\ &= -2K_\mathrm{m}\frac{u_0 - u_r}{R^2}\end{aligned} \tag{2.20}$$

$u_0 - u_r$ is the difference (wake deficit) between the free flow velocity u_0 above the wind farm and the residual wind speed u_r at the wind farm wake-centre line. Equation 2.14 is now simplified introducing the wake decay rate α.

$$\frac{du_r^2}{dx} = \underbrace{\frac{CK_\mathrm{m}}{R^2}\left(\frac{1}{f} + 1\right)}_{\alpha}(u_0 - u_r) = \alpha u_0 - \alpha u_r, \tag{2.21}$$

with here: $C = 4$ and $f \gg 1$

In this symmetric bulk approximation it is assumed that the turbulent momentum influx from aloft is the same as from below. In reality this is not the case. This is why the geometric factor C is smaller than 4 in reality and should at least be halved. Also the lateral inflow of turbulent momentum flux is primarily responsible for the shape of the wind farm wakes, i.e. shaping and shifting the outer boundary of the wind farm wake. Therefore, we assume a minimum influence of lateral influx at the wake-centre line. Hence, a factor $C = 1$ is considered in this study.

We continue to find an approximate solution of Eq. 2.21:

$$\frac{du_r^2}{dx} = 2u_r\frac{du_r}{dx} = \alpha u_0 - \alpha u_r$$

Rearranging and moving dx to the other side

$$\iff du_r = \left(\frac{\alpha u_0}{2u_r} - \frac{\alpha}{2}\right)dx \tag{2.22.1}$$

the next step is integrating over du_r on the left and over dx on the right. However:

Equation 2.22.1 is the difference form of a non-homogeneous non-linear differential equation (DE) of first order. The solutions u_r^hom of the corresponding homogeneous DE are of the form:

$$u_r^\mathrm{hom} = \pm\sqrt{\alpha u_0 x} \tag{2.22.2}$$

which actually is realistic: the reduced wind speed u_r increases by the square-root of the horizontal distance x – quite similar to the vertical development of a turbulent boundary layer or an internal boundary layer in heterogeneous terrain (Garratt, 1987; Garratt, 1994b; Hanna, 1987). However, a particular solution of the non-homogeneous DE 2.21 could not be found. In order to find an approximated solution, u_r is treated as a constant on the right-hand side of Eq. 2.22.1 and the simplified DE is solved in the following continuing from Eq. 2.22.1.

$$\iff u_r = \left(\frac{\alpha u_0}{2u_r} - \frac{\alpha}{2}\right)x + c$$

A short assessment of the order of magnitude assures that the introduced error by treating u_r as a constant for the integration step, is small, using observed wind farm wake lengths up to 60 km (Platis et al., 2018; Siedersleben et al., 2018). It is assumed that the change of the velocity gradient along x is small (with the velocity gradient in the order of $\frac{\Delta u}{\Delta x} = -\frac{u_0 - u_r(0)}{60000\,\mathrm{m}} \approx -\frac{1}{10000}\,\mathrm{s}^{-1}$), which

is several orders of magnitude smaller than the Reynolds shear stress terms or its gradient approximation wrapped in α. Let us now work with this simplified equation, where we focused on integrating u_r over du_r and neglected any dependency of u_r over small dx (considering a wind farm wake length of at least 40000 m). Thus assuming that the solution of 2.22.1 is carried by solving for u_r by solely integrating over du_r and neglecting its dependency over dx, treating the latter dependency as quasi-constant.

Rearranging again and multiplying with u_r

$$\iff u_r^2 + \frac{\alpha u_r x}{2} - c u_r - \frac{\alpha u_0 x}{2} = 0$$

rewrite as a quadratic equation

$$\iff u_r^2 + u_r\left(\frac{\alpha x}{2} - c\right) - \frac{\alpha u_0 x}{2} = 0 \qquad (2.22.3)$$

This quadratic equation has two solutions:

$$u_{r_{1,2}}(x) = \frac{1}{2}\left(\left(c - \frac{\alpha x}{2}\right) \pm \sqrt{\left(\frac{\alpha x}{2} - c\right)^2 + 2u_0 \alpha x}\right) \qquad (2.23)$$

While only the positive solution is physically relevant, resulting in positive wind speeds, c can now be determined using initial boundary conditions, i.e. for $x = 0$. The initial conditions can be measured, calculated or a theoretical value can be taken, e.g. $u_r(0) \approx 0.3u_0$ using Betz law (Betz, 1920), if applicable, resulting in $c = 0.3u_0$ (e.g. behind a single wind turbine). For the wind farm wakes used in this study, the values shown in Table 2 are used.

Equation 2.23 describes the residual wind speed u_r at each position x along the wake-centre line. The wind-deficit decay rate α, with K_m the momentum transfer coefficient, which will be assumed constant over x.

The predicted wake length is an important parameter that serves as quality control for any wake model. The wake length depends, aside of the horizontal wind speed at hub height, primarily on the thermal stability (McKay et al., 2012). As such, the SWIFFR model also has to work for different thermal atmospheric stabilities. The atmospheric stability can be implemented in the same way as in the EFFWAKE model as shown in Eq. 2.6. We assume that Eq. 2.6 is applicable for a WTs with hub heights $h = 90$ m.

The SWIFFR model is similar to the EFFWAKE model in the way the wake is treated and simplified. However, the EFFWAKE uses a Lagrangian point of view, solving Term I and Term VII of Eq. 2.8, while the SWIFFR model follows an Eulerian approach by solving for a stationary solution of Eq. 2.8, in particular, using Term II and Term VII.

2.3 Similarity to the Frandsen model

The square-root function of the SWIFFR model, Eq. 2.23, is similar to the Frandsen et al. (2006) model in regard of the proposed wind farm wake shape. The model handles a regular array geometry with straight rows of wind turbines and equidistant spacing between units in each row and equidistant spacing between rows (Frandsen et al., 2006), as does the SWIFFR model. The Frandsen model can be utilized to get a wind farm wake shape by using an effective wind farm thrust coefficient C_T^*, a wind farm parameter, instead of the rotor diameter D, and an effective wake expansion coefficient k, the latter two can be written as single parameter k^*:

$$\frac{u_r}{u_0} = \frac{1}{2}\left(1 + \sqrt{1 - \frac{2C_\mathrm{T}^*}{1 + 2k^* x}}\right) \qquad (2.24)$$

The normalisation wind speed u_0 is the free stream velocity corresponding to the first measurement, closest to the wind farm, which is presumably the velocity in the inflow, at the time of the measurement.

While the Frandsen model is a popular representative of a bottom-up model and the SWIFFR model constitutes a top-down approach, resulting in a similar equation, a comparison of the two models is shown in Section 4. The differences and commonalities of the two models will be discussed in Section 6.

3 Data treatment and model setup

3.1 In-situ wake data

The airborne-measured wind farm wake data from the WIPAFF project are accessible to the community via the PANGAEA database (Bärfuss et al., 2019; Lampert et al., 2020). The data used in this particular study was measured on August 8, 2017. Three measurement flights (#30, #31, #41) collectively contain seven wind farm wakes behind four different wind farms, Amrumbank West (AW), Nordsee Ost (NO), Meerwind Süd/Ost (MSO), and Gode Wind I/II (GW I/II) are used in the following. An overview of all flights is given in Platis et al. (2018).

The measurements were performed with the research aircraft Dornier Do-128 of the Technische Universität of Braunschweig. It is equipped among others with sensors for temperature, humidity, pressure, and wind components, sampling with a frequency of 100 Hz. Details about the measurement devices can be found in Lampert et al. (2020). The airspeed of the aircraft during the measurements flights was 66 m s^{-1}.

Figure 2 shows an exemplary measurement of the horizontal wind field u_hor normalised by the free, undisturbed flow velocity u_f, around and in the wake of the wind farm cluster AW/NO/MSO. The main wind direction is along the x-axis. To determine u_f, the mean wind speed is determined to the left and right of the wind farm cluster for each flight leg (straight part of the flight track) at various distances x and a minimum distance of about four kilometres from the adjacent wakes.

The flight track is indicated by a black solid line. The dashed black line is following the wake minimum

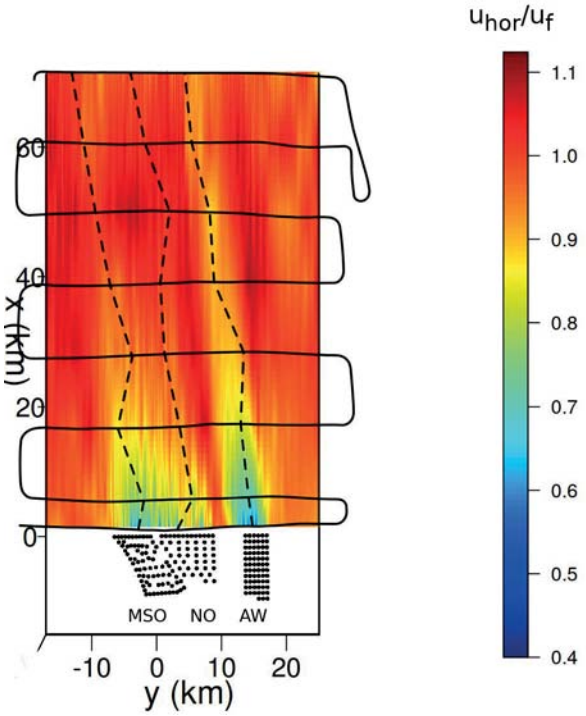

Figure 2: Normalised horizontal wind speed from an exemplary measurement (flight #31) behind the three wind farms Amrumbank West (AW), Nordsee Ost (NO), and Meerwind Süd/Ost (MSO) with eastern wind direction. The data is linearly interpolated between flightpaths in x-direction. The flight path (meander pattern) is indicated as a black solid line. The dashed black line follows the wake minimum. Black dots indicate individual WTs.

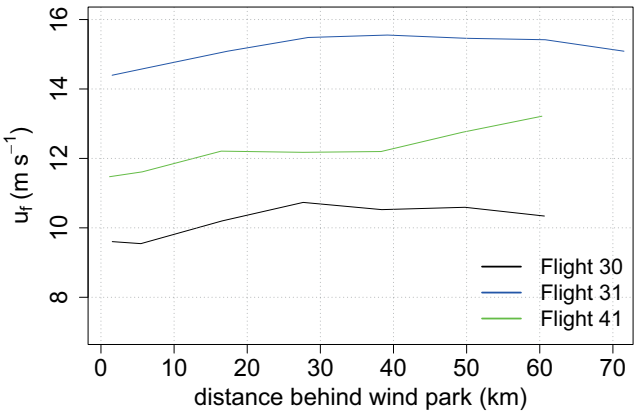

Figure 3: Free flow u_f velocities along the main wind direction next to the wind farm clusters AW/NO/MSO (flights #30 and #31) and GW I/II (flight #41).

where the residual wind velocity $u_r(x)$ in the wake is calculated. Along the flight path, with the wake minimum in its centre, the measurements of an ≈ 260 m section (400 data points) are averaged.

The EFFWAKE and SWIFFR models need an average wind velocity of the undisturbed atmospheric flow at hub height (u_0) as input. But since there are also free-stream velocity measurements available along the wake, the normalisation velocity at each distance x is set to be $u_f(x)$, instead of the incoming wind speed u_0 in front of the wind farm, throughout this study (s.a. Figure 3). This has been applied to both models, and increases the prediction accuracy, since the wind field is slightly changing over the time span of the measurements due to meso-scale effects (s.a the slight wind velocity gradient in Figure 2).

For a successful analytical solution only one more parameter aside u_f or u_0 is needed; the friction velocity u_*. This parameter has been directly taken from Table 4 ($u_{*\mathrm{FINO}}$) from Platis et al. (2020a) for the respective flights which has been measured either by the FINO 1 or the FINO 3 mast in the German Bight. Platis et al. (2020a) calculated $u_{*\mathrm{FINO}}$ using the direct method (calculation by the vertical fluxes of horizontal momentum).

3.2 EFFWAKE

The EFFWAKE model relies on a separation layer Δz. This separation height is not determinable from the measured data and is a function of stability, wind farm geometry and atmospheric boundary conditions, e.g. a possible inversion near the hub height (Platis et al., 2020a). Therefore, aside different exponential fits with different Δz, an exponential best fit of the EFFWAKE model is shown in Section 4. The fit is done the same way as implemented in Platis et al. (2020a). Equation 3.1 uses a wind deficit decay rate α_{Ebf} that fits best to the in-situ wind farm wake data, using the first measurement at distance $x_1 \approx 2$ km as a constraint.

$$\frac{u_r(x)}{u_f(x)} = 1 - \left(1 - \frac{u_r(x)}{u_f(x)}\right) \exp(-\alpha_{\mathrm{Ebf}} t(x)) \tag{3.1}$$

The best fit solution is the solution with the smallest root-mean-square deviation (RMSD):

$$\mathrm{RMSD} = \sqrt{\frac{1}{N}\sum_{i=1}^{N}\left(u(x)_i^{\mathrm{model}} - u(x)_i^{\mathrm{meas}}\right)^2} \tag{3.2}$$

N is the number of averaged wake measurements per wake, $u(x)_i^{\mathrm{model}}$ and $u(x)_i^{\mathrm{meas}}$ are the modelled and the measured residual wind velocities in the wake.

The time dependency in Eq. 3.1 is solved by substituting $t(x_i)$:

$$t(x_i) = \frac{x_i}{u_f(x_i)} \tag{3.3}$$

which is approximately the travel-time of an air parcel to position x_i outside of the wake taking into account slight variations in the mean wind speed in the incoming flow. This systematically introduces an error in the model which decreases with distance x, as the wind deficit

Table 1: Determination of the geometrical factor f from wind farm dimensions considering the main wind direction in the SWIFFR model.

Wind farm	lateral extent [m]	vertical extent [m]	f [–]
AW	2400	60	40
NO	3000	60	50
MSO	2500	60	42
GW I/II	5000	60	80

$(u_f - u_r)$ decreases, and the wind speed in the wake is getting closer to the free flow velocity u_f.

Starting from the wind deficit decay rate of the EFFWAKE model:

$$\alpha_{\mathrm{Ebf}} = \frac{K_{\mathrm{m}}}{\Delta z_{\mathrm{bf}}^2} = \frac{\kappa u_* (h + \Delta z_{\mathrm{bf}})}{\Delta z_{\mathrm{bf}}^2}, \tag{3.4}$$

which is a computed best-fit (least-square fit) wind-deficit decay rate α_{Ebf}. From there, Δz_{bf} is solved for each wind farm wake by:

$$\Delta z_{\mathrm{bf}} = \frac{1 + \sqrt{1 + 4\alpha_* h}}{2\alpha_*}, \text{ with } \alpha_* = \frac{\alpha_{\mathrm{Ebf}}}{\kappa u_*}, \tag{3.5}$$

which is then used for comparison and discussion.

3.3 SWIFFR

In contrast to the EFFWAKE model, the proposed analytical solution in this study is using a fixed distance R (the rotor blade length) to the vertical wake boundary, measured from hub height. However, aside the free flow velocity u_f the SWIFFR model needs an additional parameter c which is derived from initial conditions (s.a. Section 2.2). These conditions were estimated, and the exact value is taken that the analytical solution passes through the measurement at distance $x_1 \approx 2000\,\mathrm{m}$. The wind farm capacity is also considered at the time of the measurement to check for plausibility (www.energy-charts.info).

The geometrical factor f used in the SWIFFR model for the respective wind farms by calculating f from the cross-section of the wind farm perpendicular to the main wind direction:

$$f = \frac{\text{lateral extent from wake centre line}}{\text{vertical extent from hub height}} \tag{3.6}$$

The resulting values are shown in Table 1.

3.4 Comparison with the Frandsen (2006) model

For the comparison of the Frandsen and the SWIFFR model parameters from Table 2 are used. The thrust coefficient C_T^* is set to match $u_r(0)/u_f$ from Table 2. The normalised wake widening coefficient k^* is set to coincide with $u_r(60000)/u_0$ of the SWIFFR model. For this comparison the SWIFFR model is set up using Eq. 2.23 with $u_0 = u_f(0)$ assuming that the initial wind velocity in front of the wind park $u_0 \approx u_f(0)$. Keep in mind that $u_f(0)$ is measured at around 500–600 m in the wake and cannot be measured at $x = 0\,\mathrm{m}$ due to practical and safety reasons.

In this comparison the SWIFFR model is used as sole prediction tool as the Frandsen model as well. Hence, assuming constant wind conditions and no adjustment of the free flow wind velocity $u_f(x)$ along the wake.

4 Results

The results of the wind farm wake analysis is given in the following by looking into three flights from the WIPAFF campaign 2017. The data for flights #30 and #31 were captured on August 8, 2017. Flight #30 in the morning from 08:30 to 12:30 UTC, flight #31 in the afternoon from 13:00 to 17:00 UTC. Those two flights are especially interesting, since they provide measurements throughout a whole day as the marine boundary layer evolves. These two flights also enable a comparison of three wind farm wakes with the same inflow conditions, due to the vicinity of the three wind farms.

Table 2 lists all model parameters for the presented flights and wind farm wakes. The EFFWAKE model is represented by the exponential best fit in the table, from which a Δz_{bf} has been back-calculated assuming the friction velocity u_* associated with this flight (s.a. Section 3.1) and the present atmospheric conditions. The wind deficit decay rate α has also been normalised by the mean inflow conditions, calculated from u_f (s.a. Figure 3). This way the wind deficit decay rate is also more tangible.

4.1 Flight #30

For flight 30 the atmospheric conditions were similar to flight #31, but the stratification was slightly less stable. The friction velocity u_*, taken from Platis et al. (2020a), was $0.22\,\mathrm{m\,s^{-1}}$, the average free stream velocity was $\overline{u_f} = 10.2\,\mathrm{m\,s^{-1}}$ with easterly wind from 80°. The Amrumbank West wind farm was operating between 42–76 % capacity during the time span of the measurements (www.energy-charts.info). During flight #30 the thermal stratification shows an almost neutral gradient, with a thermal inversion at 160 m above sea level. Thus, with the inversion at 160 m, the rotor blade area remains completely in the neutral layer (Platis et al., 2020a). Figure 4 shows the measurements behind the wind farms and the analytical solutions for the SWIFFR and EFFWAKE model. The latter is shown for different Δz and also for the best-fit wind deficit decay rate.

Figure 4 shows the in-situ measurements, the SWIFFR model solution (thick black line), the EFFWAKE best fit (red dashed line) and EFFWAKE solution for different Δz (grey-shaded lines).

Table 2: Model parameters and root-mean-square deviations (RMSD) of the EFFWAKE and SWIFFR model for all presented cases. With $u_r(0)/u_f(0) = c$ and C_T the thrust coefficient of the wind farm derived from the Frandsen model.

Flight No.	**Wind farm**	u_* [m s^{-1}]	α_{Ebf} [h^{-1}]	$\alpha/\overline{u}_f$ [km^{-1}]	Δz_{bf} [m]	$c\|_{x=0}$ [–]	C_T [–]	Π [–]	RMSD · 10^3 [m s^{-1}]
EFFWAKE (best fit)									
30	AW	0.22	1.26	0.034	320	0.73	0.45	0.33	41
30	NO	0.22	2.76	0.075	170	0.59	0.49	0.29	40
30	MSO	0.22	2.26	0.061	200	0.78	0.39	0.30	27
31	AW	0.29	1.40	0.026	370	0.61	0.50	0.31	41
31	NO	0.29	3.40	0.062	180	0.63	0.49	0.31	38
31	MSO	0.29	3.60	0.066	180	0.70	0.45	0.32	22
41	GW I/II	0.21	1.00	0.022	430	0.68	0.48	0.33	39
SWIFFR			α [h^{-1}]		R [m]				
30	AW	0.22	13.5	0.365	60	0.65	0.45	0.29	33
30	NO	0.22	13.4	0.362	60	0.55	0.49	0.27	45
30	MSO	0.22	13.4	0.365	60	0.73	0.39	0.28	17
31	AW	0.29	17.8	0.325	60	0.35	0.50	0.18	47
31	NO	0.29	17.7	0.322	60	0.55	0.49	0.27	21
31	MSO	0.29	17.6	0.321	60	0.65	0.45	0.29	25
41	GW I/II	0.21	9.0	0.200	60	0.60	0.48	0.29	37
Frandsen					$k^* \cdot 10^5$ [m^{-1}]		C_T^*		
30	AW				6.25	0.66	0.45	0.30	39
30	NO				5.31	0.57	0.49	0.28	45
30	MSO				7.10	0.74	0.39	0.28	20
31	AW				3.11	0.50	0.50	0.25	44
31	NO				4.70	0.57	0.49	0.28	22
31	MSO				5.50	0.65	0.45	0.29	21
41	GW I/II				3.40	0.60	0.48	0.29	47
super-SWIFFR				Λ [km^{-1}]			C_T^*		
30	AW			0.343			0.45	0.28	37
30	NO			0.343			0.49	0.28	44
30	MSO			0.343			0.39	0.28	19
31	AW			0.343			0.50	0.28	70
31	NO			0.343			0.49	0.28	23
31	MSO			0.343			0.45	0.28	23
41	GW I/II			0.343			0.48	0.28	62

4.2 Flight #31

For flight #31 (s.a. Figure 5) of the WIPAFF campaign, the same atmospheric parameters as calculated in the flight evaluation by Platis et al. (2020a) are used: $u_* = 0.29\,\mathrm{m\,s^{-1}}$ and an average free stream velocity of $15.1\,\mathrm{m\,s^{-1}}$ with an easterly wind from 80°. According to the temperature profile, measured in the vicinity of the wind farm cluster, a thermally stable layer was present up to approximately 100 m above sea level (Platis et al., 2020a). The hub height of the turbines of the wind farm cluster is around 90 m, with a rotor diameter of 120 m; thus, the total turbine height reaches 150 m. In this case, with the detected surface layer up to 100 m, the turbines are in the stable layer, but the rotor blades do cut into the neutral layer above (Platis et al., 2020a). During the time span of the measurements the wind farm operated at a capacity between 90–95 %. This results in a very low residual wind velocity at the beginning of the wake, especially visible at the Amrumbank West wind farm (Figure 5a).

4.3 Flight #41

In contrast to the preceding two measurement flights, flight #41 (Figure 6) does not allow an inter-comparison of wind farm wake behaviour for the same atmospheric boundary conditions, since the wind farms Gode Wind I and II are overflown in sequence by the prevailing atmospheric flow. An evaluation of this flight still serves as a comparison of the EFFWAKE and SWIFFR models. Flight #41 took place on October 15 2017 between approximately 12:00 and 16:00 UTC with dominating southerly wind direction (190°) with an average wind speed of $12\,\mathrm{m\,s^{-1}}$. The thermal gradient indicates a stable stratification from the sea surface up to hub height with half the rotor plane then being in a continuing neutral to slightly stable thermal atmospheric stratification

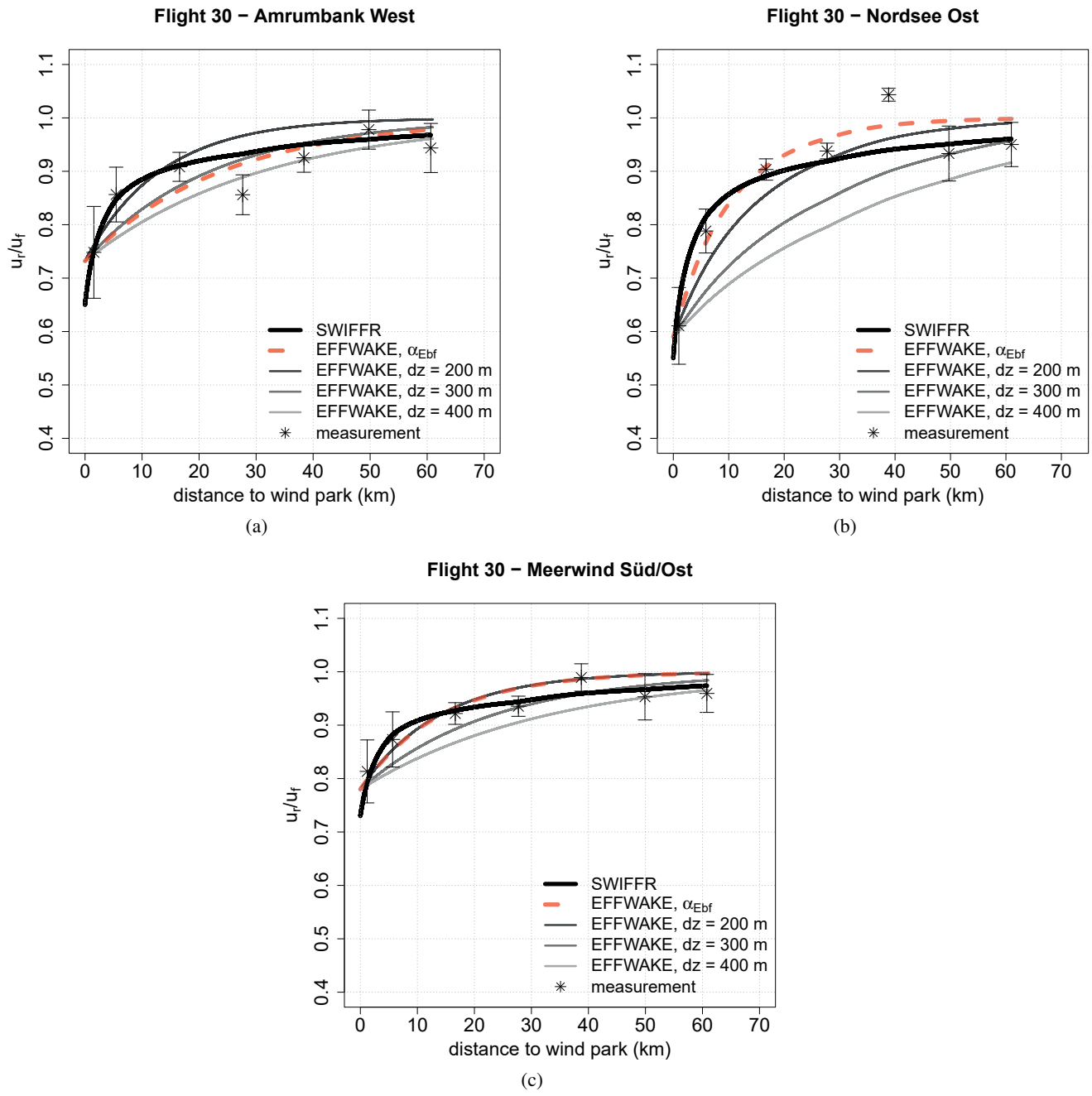

Figure 4: Evaluation of the three wind farm wakes AW (a), NO (b) and MSO (c) for flight #30. Same atmospheric boundary conditions are assumed for all three wakes, due to the vicinity of the three wind farms.

up to a beginning inversion at 400 m. A friction velocity $u_* = 0.21\,\mathrm{m\,s^{-1}}$ has been calculated from FINO 1 data as done by Platis et al. (2020a).

Figure 6a shows two different wind velocities left and right of the wind farm wake. This makes it difficult to define a free flow velocity. Such an uncertainty may impact the model accuracy, and concretely the normalisation of the calculated residual wind speeds.

4.4 Super-SWIFFR derivation

Figure 7 shows the comparison of the Frandsen model, the SWIFFR models as presented in Eq. 2.23 and a fully parametrised version (super-SWIFFR) which derivation is shown below. Observing the results of the Frandsen and SWIFFR solution in Figure 7, both models provide a square-root-shape result and are derived from momentum equations. The respective predictions of the two models coincide, except at Flight #31 – AW. Here, the initial wind deficit is greater than 50 %. To overcome this issue, for this specific wake the Frandsen solution is shifted by 620 m.

The wind farm thrust coefficient C_T^* and wind farm wake widening factor k^* [$\mathrm{m^{-1}}$] that were used for each wake modelling are shown in each subplot.

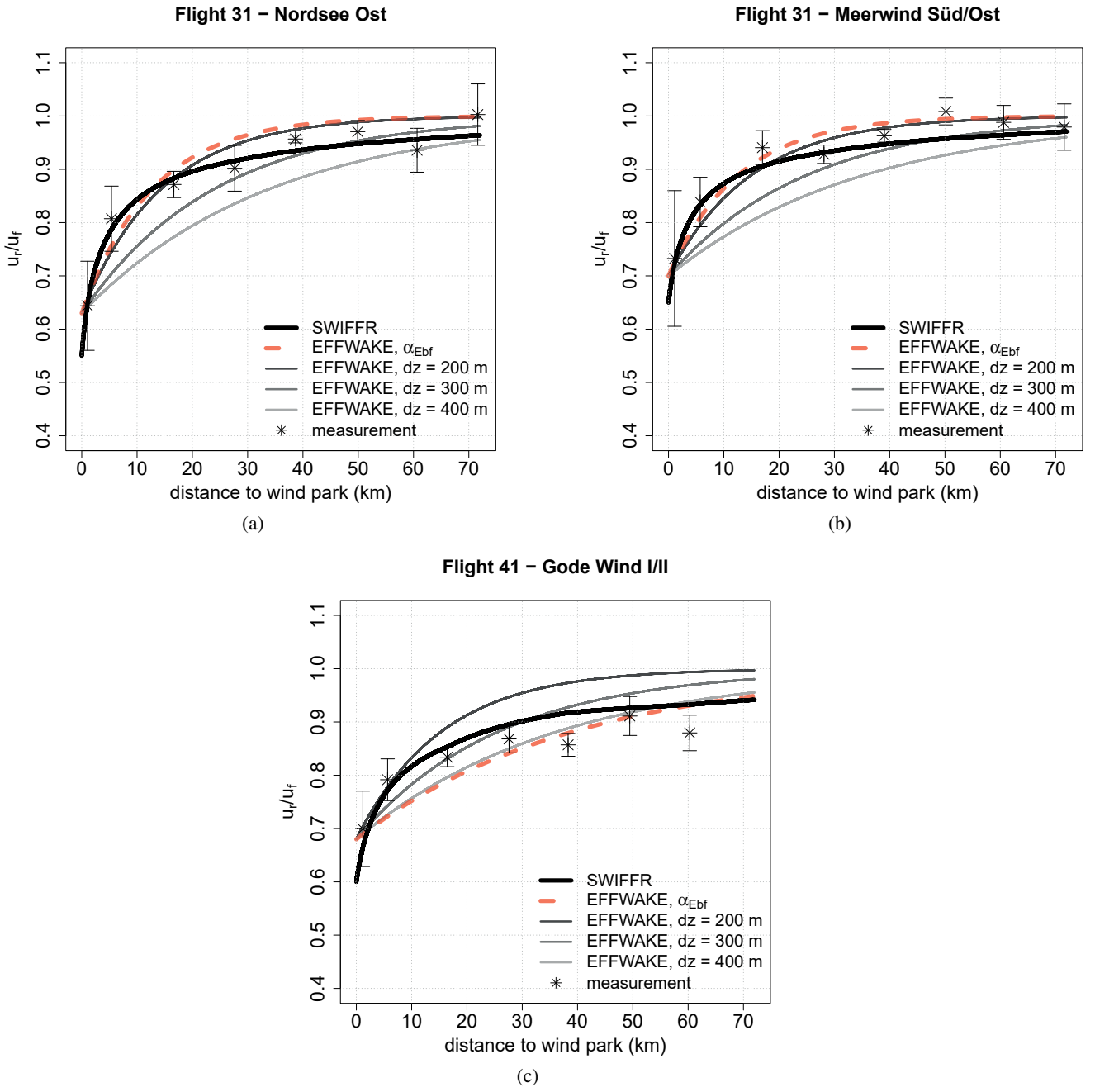

Figure 5: Evaluation of the three wind farm wakes AW (a), NO (b) and MSO (c) for flight 31.

Considering the overlapping results of the Frandsen and SWIFFR solution, the data can be used to derive an empirical relation between $c|_{x=0}$ and the thrust coefficient C_{T}^{*}. Since both parameters negatively correlate (a high thrust coefficient is expected for a low c-value) the product Π(s.a. Table 2) is checked for proportionality, i.e. in its simplest form a constant relationship:

$$\Pi_i = c_i|_{x=0} \cdot C_{\mathrm{T}i}^{*} = \text{constant} \approx 0.28 \qquad (4.1)$$

With i each of the seven flights and neglecting #31 AW, the average product seems to be nearly constant at $\Pi = 0.28$.

Using this first parametrisation, the modified SWIFFR solution utilising the thrust coefficient derived from the Frandsen solution, can then be calculated using:

$$u_r(x) = \frac{1}{2}\left(\left(\frac{\Pi u_0}{C_{\mathrm{T}}^{*}} - \frac{\alpha x}{2}\right) + \sqrt{\left(\frac{\alpha x}{2} - \frac{\Pi u_0}{C_{\mathrm{T}}^{*}}\right)^2 + 2u_0\alpha x}\right) \qquad (4.2)$$

For the final simplification, the a priori unknown parameter α is substituted. Therefore, Λ is introduced:

$$\Lambda = \frac{\overline{\alpha_i}}{\overline{u_{fi}}} \approx 0.343. \qquad (4.3)$$

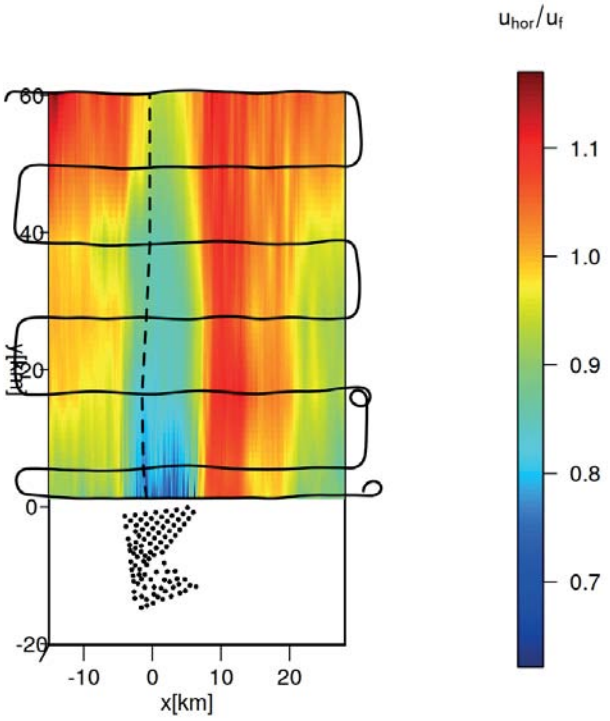

(a)

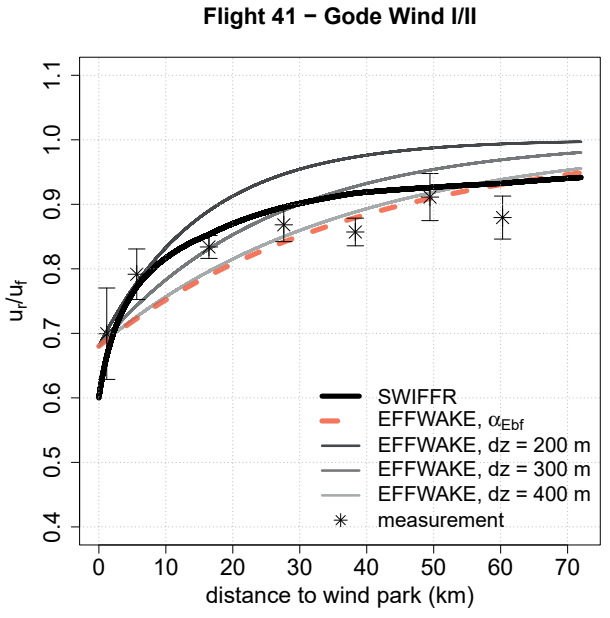

(b)

Figure 6: Evaluation of the common wake of Gode Wind I and II (flight #41). (a) In-situ wake measurements from the WIPAFF campaign. (b) Comparison of the analytical solutions from EFFWAKE and SWIFFR along the wake-minimum line indicated by the dashed line in (a).

Since Λ is the average of a normalised parameter (excluding GW I/II), its insertion into the final equation needs to be accompanied by a velocity: the free stream velocity at hub height u_f, preferably in front of the wind farm u_0. The super simplified version then becomes:

$$u_r(x) = \frac{1}{2}\left(\left(\frac{\Pi u_0}{C_\mathrm{T}^*} - \frac{\Lambda u_0 x}{2}\right) + \sqrt{\left(\frac{\Lambda u_0 x}{2} - \frac{\Pi u_0}{C_\mathrm{T}^*}\right)^2 + 2u_0^2 \Lambda x}\right) \tag{4.4}$$

Dividing by u_0 yields the relative residual wind velocities behind the wake, depending only on the thrust coefficient C_T^*:

$$\frac{u_r(x)}{u_0} = \frac{1}{2}\left(\left(\frac{\Pi}{C_\mathrm{T}^*} - \frac{\Lambda x}{2}\right) + \sqrt{\left(\frac{\Lambda x}{2} - \frac{\Pi}{C_\mathrm{T}^*}\right)^2 + 2\Lambda x}\right) \tag{4.5}$$

A graphical comparison of Eq. 4.5 is given in Figure 7 (blue line). Worth noting is the solution for the GW I/II wind farms that is only about maximum 5 % off, despite using Λ that is 58 % larger than $\frac{\alpha}{u_f}$. The special status of the GW I/II measurements is explained in Section 4.3.

5 Limitations

Emeis (2022) compiled a list of limitations that top-down models still have to battle with. This list consists of the following assumptions:

1. indefinite lateral extent of the wind farms,
2. stationarity,
3. horizontal homogeneity,
4. wind turbines are small compared to the boundary layer height,
5. governing equations from different boundary-layer descriptions fit together,
6. vertical turbulent momentum flux is shear-driven only.

Since the Frandsen model is a bottom-up model and has no intended link to atmospheric boundary conditions, this model will not be regarded in the following assessment.

5.1 Indefinite lateral extent of wind farms

This is an assumption that is made in the EFFWAKE model. The SWIFFR model approach is different and the model is able to incorporate the lateral extent of a wind farm into its turbulent momentum flux parametrisation (s.a. Eq. 2.18). While for large wind farms the effect of lateral momentum flux is negligible, the formalism allows to describe single wind turbine wakes that can be considered ‘wind farm’ wakes with a lateral extent of one rotor radius R from the wake centre line.

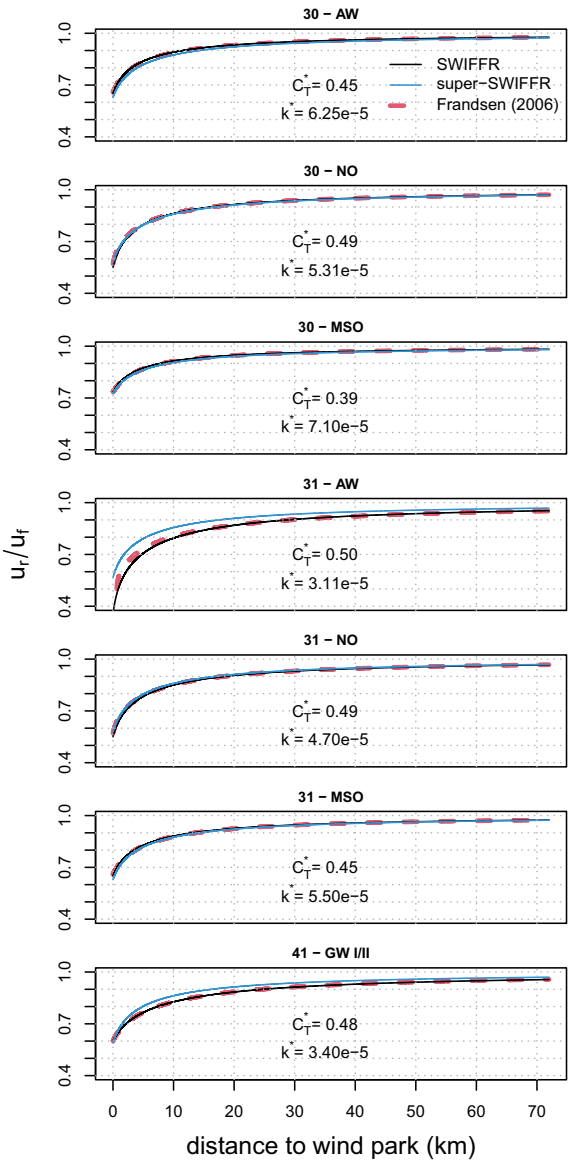

Figure 7: Comparison between the model by Frandsen et al. (2006) and two SWIFFR models; one 'stock' model and one parametrised using dependencies derived from Table 2. While SWIFFR uses a top-down approach, the Frandsen model is a typical representative of a bottom-up model. Despite the difference in their respective derivation, the SWIFFR and Frandsen model predictions coincide, except Flight #31 – AW, where the initial wind deficit is exceeding 50 %.

5.2 Stationarity

EFFWAKE and SWIFFR, both assume steady-state conditions, neglecting synoptic changes and Coriolis effects. Since off-shore atmospheric conditions do not change rapidly, it can be argued that a quasi-non-steady-state solution can be computed using a series of steady-state computations with adjusted input parameters (e.g. mean inflow velocity, friction velocity u_*, wind deficit decay rate α) that resemble the change of the boundary conditions.

5.3 Horizontal homogeneity

The simplified steady-state solutions of analytical models, e.g. the present EFFWAKE and SWIFFR models, are not designed to handle heterogeneities. Any surface patterns that can cause inhomogeneity, like a coast line or a neighbouring wind farm, must not negate the steady-state model assumptions. Therefore, for the model to be applied, the distance to the next surface inhomogeneity should be a manifold of the characteristic length of the wind farm.

Wind turbine spacing is also a factor that influences wind farm efficiency but can not be directly used by the top-down models. Both models describe the recovery of a wind velocity depression, thus EFFWAKE and SWIFFR consider the wind farm and its respective wind turbine spacing as a 'black box'-momentum sink.

5.4 Wind turbine height compared to surface layer height

In the course of the models derivations some assumptions about the vertical wind profiles are made. On the one hand the top-down models assume the hub height of the wind turbines to be at the edge of the surface or Prandtl layer (requirement for Eq. 2.6 to be valid). On the other hand, it is assumed that the mean wind velocity does not further increase above hub height nor decrease significantly below $h - R$. With increasing wind turbine heights in the future, the validity of these assumptions needs to be evaluated.

5.5 Governing equations from different boundary-layer descriptions fit together

See above.

5.6 Shear-driven vertical turbulent momentum flux

Emeis (2022) summarises the following: Generally, the friction velocity is linked to vertical wind shear when closing the full set of equations of motion. This means that vertical profile laws and also the geostrophic drag law, which involve the friction velocity, are based on the presence and dominance of shear-driven turbulence, which in turn is responsible for vertical turbulent momentum fluxes. This assumption leads to problems in strongly stable conditions where well-defined turbulence is no longer present, and in strongly unstable conditions where thermally driven turbulence dominates the shear-driven turbulence (see, e.g., Stull (1988)).

However, both presented analytical top-down models are capable of mapping very long wind farm wakes, typically found in very stable conditions.

6 Discussion and conclusions

Provided the EFFWAKE and SWIFFR models both use the same atmospheric input parameters (u_*, u_f) the newly proposed SWIFFR model can stand out with an easy to determine analytical fit for given atmospheric conditions. The major disadvantage of the EFFWAKE model is the dependency of a precise Δz, which is usually impossible to determine. Also Δz is a parameter that is a function of turbine spacing and atmospheric conditions, since it is essentially the height of the internal boundary layer above a wind farm.

The SWIFFR model gives a good prediction with less unknown variables, derived from the flow-governing equations (top-down approach). The initial conditions need to be known for both models and can be calculated using established bottom-up engineering models. These bottom-up models formulate the wake-governing equation starting from the behaviour of a single wind energy turbine, usually modelled as a rotating disk. Alternatively to calculating initial conditions, empirical values can be used for a quick assessment. Or, as for the validation of this model in this study, measured data can be used. In practice, this could be sonic anemometers on top of wind turbines or, maybe the better choice, forward looking lidar measurements on top of wind turbines scanning the inflow and the wake. This means that the SWIFFR model, for a distinct wind deficit, computes a development of the wind recovery, based on relatively easy to obtain parameters: the (average) radius of the rotor plane R of the wind turbines in the wind farm, the friction velocity u_* and the mean wind speed u_0 or, if applicable, $u_f(x)$ at hub height. Additionally, it was shown that the SWIFFR model can be altered to use a wind farm thrust coefficient C_T as an input variable, making the model independent of initial wake deficit measurements. For this study the thrust coefficients determined by the well established Frandsen model have been used. The constant $\overline{\Pi} \approx 0.28$ is expected to be independent of atmospheric stability, since it is derived from the initial wind farm wake deficit that we consider independent of thermal stratification. Equation 4.2 represents the first simplification of the SWIFFR model by removing c from the equation. The next and final simplification consists of embedding an average, normalised wind deficit decay rate Λ. For the present cases the gained simplification is worth the small loss of accuracy. Λ indirectly contains informations like atmospheric stability, friction velocity u_* and wind turbine spacing. Thus, Λ is not to be understood as a value that will work in all circumstances, and should be further investigated. But Table 2 and Figure 7 suggest that a variation of $\Lambda \pm 10\,\%$ still provides solutions with acceptable RMSDs for a fairly wide range of u_* values.

Table 2 shows that the SWIFFR model uses roughly identical wind deficit decay rates α for the different wind parks for the evaluated flights. They only differ slightly due to the f-parameter, a parameter which is given by the wind farm geometry. This behaviour is expected, since we argue that the wind deficit decay rate is largely depending on the atmospheric boundary conditions (stability and mean incoming wind velocity) which are the same for the wind farms AW, NO, and MSO in flight #30 and again for flight #31, respectively, since the three wind parks are clustered together. Thus, Table 2 indicates that the wind deficit decay rates α mostly change with the friction velocity u_* or a change in the mean flow velocity u_0 at the inflow. The normalised wind deficit decay rate $\alpha/\overline{u}_f$ suggests a correlation to the incoming mean flow velocity. In simple terms, $\alpha/\overline{u}_f$ is a measure of turbulent influx per wind velocity (e.g. at the inlet). Mathematically, u_* directly influences α. Physically, higher wind velocities may also lead to higher shear stress above/around a wind farm and therefore also impact α. At the latest, when normalising α and yielding Λ.

Also note, that the SWIFFR model was not stability corrected, i.e. no z/L-correction as in Eq. 2.6 was implemented, at this point of the data evaluation. Using the measured values for u_* and u_0 (or $u_f(x)$) was sufficient for the SWIFFR model to fit to the wind farm wake measurements. Thus, it is hard to argue which parameter is the dominating factor defining the behaviour of α, having only the available data (s.a. Table 2). The super-SWIFFR solution uses Λ, a parameter that incorporates stability affected behaviour of the wake. But to proof this, further studies and more data is needed.

Regarding the model accuracy, both models provide a similar accuracy, considering the EFFWAKE best fit. However, the EFFWAKE best fit can only be modelled to the data, there is no possible way of knowing Δz for the different wind parks in different atmospheric conditions, also illustrated in Figure 4-6. See also the varying Δz_bf in Table 2 for the different wind parks, yet the same atmospheric conditions. Well pictured in Figure 5, where the best corresponding best fit Δz values are approximately halved when the wind farms AW and NO are compared. Thus, Δz might be considered more a geometrically influenced parameter. At this point, the EFFWAKE model lacks in terms of a prediction model, since there is no source on how to choose Δz for different wind farm configurations.

The SWIFFR model is additionally compared to the Frandsen model that is used to calculate the wind deficit behind a single wind turbine, but is also used to calculate the wind deficit behind wind farms. Both square-root-shape models are derived from momentum conservation equations. Also, both models use at least one parameter that is not easily calculated: the wake widening coefficient k or k^* in the Frandsen model and the wind deficit decay rate α in the SWIFFR model. Despite the difference in their respective derivation, both models generally coincide and predict identical wake lengths. This indicates that the SWIFFR model can be used to determine and predict wind farm wake lengths in a similar way as the Frandsen model. It simply uses other input parameters. In contrast to the wind farm (wake) properties that are used as inputs in the Frandsen model, the SWIFFR

model uses atmospheric flow properties. Therefore, the SWIFFR model has the potential to be used for wind and weather forecasting, i.e. for computations whenever effects of changing atmospheric conditions are of interest.

7 Outlook

The EFFWAKE and SWIFFR model provide a quick and simple way to model a wind-farm wake using only few input parameters. In the presented cases the SWIFFR model can give a prediction of the wake length, whereas the EFFWAKE model only works applying a best fit to observational data, since Δz is a priori unknown. The obtained accuracy from the beginning of the wake till the end of the wake is more or less comparable (according to the RMSD). Yet, the SWIFFR model solely provides an actual prediction of the wind-farm wakes, so does the Frandsen model. While the latter model uses wind turbine properties to describe the wake, the SWIFFR model relies on atmosphere-related parameters. Thus, the SWIFFR model is suited for weather forecasting models that already utilise the friction velocity and mean wind speed. The super-SWIFFR altercation of the model expands the model applicability further by providing a possibility to use the model with a common wind farm modelling parameter (only), the thrust coefficient C_T. Thus, Eq. 4.5 combines an element of a bottom-up approach (thrust coefficient), and through the parametrisation of atmospheric data, elements of a top-down approach (u_*, u_0, K_m). To further specify the parameters Λ and Π more studies are necessary, especially in different atmospheric thermal stabilities present.

The ease of use of the super-SWIFFR model would increase tremendously, should future investigations and data evaluations show, that the wind deficit decay rate α correlates sufficiently with the incoming mean wind velocity and a credible Λ could be retrieved. Therefore, we need reliable atmospheric measurements also to derive stability parameters for further investigations of the atmospheric thermal stability relation. Such data sets would also provide an opportunity to revisit a comparison of the SWIFFR and EFFWAKE model, since it would allow further investigations into the Δz parameter of the EFFWAKE model.

So far this model assessment is only valid with no significant inversion present. With ever-increasing wind turbine dimensions, both models need to be eventually adjusted due to this development.

Authorcontribution

Moritz Mauz derived the model formalism and the equations and evaluated the data. Frederick Höckh provided the sets of processed WIPAFF data. Bram van Kesteren contributed to the formalism. Andreas Platis, Stefan Emeis and Jens Bange added to the general discussion of the topic and added valuable input to shape this study.

Acknowledgments

The project WIPAFF was funded by the German Federal Ministry for Economic Affairs and Energy (Bundesministerium für Wirtschaft und Energie) on the basis of a decision by the German Bundestag grant number: FKZ 0325783

This open-access publication was funded by the University of Tübingen.

References

Andersen, S., J. Sørensen, S. Ivanell, R. Mikkelsen, 2014: Comparison of engineering wake models with CFD simulations. – J. Phys. Conf. Ser. **524**, 012161, 10.1088/1742-6596/524/1/012161. Content from this work may be used under the terms of the Creative Commons Attribution 3.0 licence. Any further distribution of this work must maintain attribution to the author(s) and the title of the work, journal citation and DOI. – Published under licence by IOP Publishing Ltd; 5th International Conference on The Science of Making Torque from Wind 2014, TORQUE 2014.

Antonini, E.G., K. Caldeira, 2021: Atmospheric pressure gradients and coriolis forces provide geophysical limits to power density of large wind farms. – Appl. Energy **281**, 116048, DOI: 10.1016/j.apenergy.2020.116048.

Bärfuss, K., R. Hankers, M. Bitter, T. Feuerle, H. Schulz, T. Rausch, A. Platis, J. Bange, A. Lampert, 2019: In-situ airborne measurements of atmospheric and sea surface parameters related to offshore wind parks in the German Bight. – PANGAEA, published online, https://doi.pangaea.de/10.1594/PANGAEA.902845.

Betz, A., 1920: Das maximum der theoretisch möglichen ausnützung des windes durch windmotoren. – Z. gesamte Turbinenwesen **26**, 307–309.

Businger, J.A., J.C. Wyngaard, Y. Izumi, E.F. Bradley, 1971: Flux-profile relationships in the atmospheric surface layer. – J. Atmos. Sci. **28**, 181–189, DOI: 10.1175/1520-0469(1971)028<0181:FPRITA>2.0.CO;2.

Canadillas, B., R. Foreman, V. Barth, S. Siedersleben, A. Lampert, A. Platis, B. Djath, J. Schulz-Stellenfleth, J. Bange, S. Emeis, T. Neumann, 2020: Offshore wind farm wake recovery: Airborne measurements and its representation in engineering models. – Wind Energy **23**, DOI: 10.1002/we.2484.

Djath, B., J. Schulz-Stellenfleth, B. Canadillas, 2018: Impact of atmospheric stability on x-band and c-band synthetic aperture radar imagery of offshore windpark wakes. – J. Renew. Sustain. Energy **10**, 043301, DOI: 10.1063/1.5020437.

Emeis, S., 2010: A simple analytical wind park model considering atmospheric stability. – Wind Energy **13**, 459–469, DOI: 10.1002/we.367.

Emeis, S., 2017: Wind Energy Meteorology. – Springer, Heidelberg, Germany, 144–146.

Emeis, S., 2022: Analysis of some major limitations of analytical top-down wind-farm models. – Bound.-Layer Meteor. **187**, 423–435, DOI: 10.1007/s10546-021-00684-4.

Emeis, S., S. Siedersleben, A. Lampert, A. Platis, J. Bange, B. Djath, J. Schulz-Stellenfleth, T. Neumann, 2016: Exploring the wakes of large offshore wind farms. – J. Phys. Conf. Ser. **753**, 092014, DOI: 10.1088/1742-6596/753/9/092014.

Frandsen, S., R. Barthelmie, S. Pryor, O. Rathmann, S. Larsen, J. Højstrup, M. Thøgersen, 2006: Analytical modelling of wind speed deficit in large offshore wind farms. – Wind Energy **9**, 39–53, DOI: 10.1002/we.189.

Garratt, J., 1994a: The Atmospheric Boundary Layer. – Cambridge Atmospheric and Space Science Series. – Cambridge University Press.

Garratt, J., 1994b: Review: the atmospheric boundary layer. – Earth-Sci. Rev. **37**, 89–134, DOI: 10.1016/0012-8252(94)90026-4.

Garratt, J.R., 1987: The stably stratified internal boundary layer for steady and diurnally varying offshore flow. – Bound.-Layer Meteor. **38**, 369–394, DOI: 10.1007/BF00120853.

Hanna, S.R., 1987: An empirical formula for the height of the coastal internal boundary layer. – Bound.-Layer Meteor. **40**, 205–207, DOI: 10.1007/BF00140077.

Hassan, G., Partners Ltd., 2014: Windfarmer tutorial: Introduction to windfarmer. – Technical report.

Jensen, N., 1983: A note on wind generator interaction Number 2411 in Risø-M. – Risø National Laboratory.

Katić, I., J. Højstrup, N.O. Jensen, 1987: A simple model for cluster efficiency. – In: Palz, W., E. Sesto (Eds), EWEC'86, Proceedings. Vol. 1, 407–410).

Lampert, A., K.B. Bärfuss, A. Platis, S.K. Siedersleben, B. Djath, B. Cañadillas, R. Hankers, M. Bitter, T. Feuerle, H. Schulz, T. Rausch, M. Angermann, A. Schwithal, J. Bange, J. Schulz-Stellenfleth, T. Neumann, S. Emeis, 2020: In-situ airborne measurements of atmospheric and sea surface parameters related to offshore wind parks in the German Bight. – ESSD **12**, 935–946.

McKay, P., R. Carriveau, D.S.T. Ting, T. Newson, 2012: Turbine Wake Dynamics. – IntechOpen, 10 Lower Thames Street, London, EC3R 6AF, UK.

Meyers, J., C. Meneveau, 2012: Optimal turbine spacing in fully developed wind farm boundary layers. – Wind Energy **15**, 305–317, DOI: 10.1002/we.469.

Niayifar, A., F. Porté-Agel, 2016: Analytical modeling of wind farms: A new approach for power prediction. – Energies **9**, 741, DOI: 10.3390/en9090741.

Platis, A., S.K. Siedersleben, J. Bange, A. Lampert, K. Bärfuss, R. Hankers, B. Canadillas, R. Foreman, J. Schulz-Stellenfleth, B. Djath, T. Neumann, S. Emeis, 2018: First in situ evidence of wakes in the far field behind offshore wind farms. – Scientific Reports **8**, 2163, DOI: 10.1038/s41598-018-20389-y.

Platis, A., M. Hundhausen, M. Mauz, S. Siedersleben, A. Lampert, K. Bärfuss, B. Djath, J. Schulz-Stellenfleth, B. Canadillas, T. Neumann, S. Emeis, J. Bange, 2020a: Evaluation of a simple analytical model for offshore wind farm wake recovery by in situ data and weather research and forecasting simulations. – Wind Energy **24**, 212–228, DOI: 10.1002/we.2568.

Platis, A., J. Bange, K. Bärfuss, B. Canadillas, M. Hundhausen, B. Djath, A. Lampert, J. Schulz-Stellenfleth, S. Siedersleben, T. Neumann, S. Emeis, 2020b: Long-range modifications of the wind field by offshore wind parks – results of the project WIPAFF. – Meteorol. Z. **29**, 355–376, DOI: 10.1127/metz/2020/1023.

Prandtl, L., 1904: über flüssigkeitsbewegung bei sehr kleiner Reibung. – Verhandlungen des III. Intern. Math. Kongr. Heidelberg. –Gesammelte Abhandlungen **2**, 484–491.

Siedersleben, S.K., A. Platis, J.K. Lundquist, A. Lampert, K. Bärfuss, B. Cañadillas, B. Djath, J. Schulz-Stellenfleth, J. Bange, T. Neumann, S. Emeis, 2018: Evaluation of a wind farm parametrization for mesoscale atmospheric flow models with aircraft measurements. – Meteorol. Z.**27**, 401–415, DOI: 10.1127/metz/2018/0900.

Stull, R.B., 1988: An introduction to boundary layer meteorology. – Kluwer Academic Publishers, Dordrecht, the Netherlands.

Yang, X., S. Kang, F. Sotiropoulos, 2012: Computational study and modeling of turbine spacing effects in infinite aligned wind farms. – Phys. Fluids **24**, 115107, DOI: 10.1063/1.4767727.

Zhan, L., S. Letizia, G. Valerio Iungo, 2020: Lidar measurements for an onshore wind farm: Wake variability for different incoming wind speeds and atmospheric stability regimes. – Wind Energy **23**, 501–527, DOI: 10.1002/we.2430.